Short communication

Sintering and electrical conductivity of the GdSmZr$_2$O$_7$ ceramic with and without ZnO sintering aid

Zhan-Guo Liu*, Jia-Hu Ouyang*, Yu Zhou

Institute for Advanced Ceramics, School of Materials Science and Engineering, Harbin Institute of Technology, 92 West Da-Zhi Street, Harbin 150001, China

HIGHLIGHTS

- The 1 wt.% ZnO-modified GdSmZr$_2$O$_7$ exhibits a single cubic pyrochlore-type phase.
- 1 wt.% ZnO to GdSmZr$_2$O$_7$ promotes sintering densification.
- 1 wt.% ZnO to GdSmZr$_2$O$_7$ reduces the sintering temperature by about 200 K.
- The total conductivity of GdSmZr$_2$O$_7$ is improved by the addition of 1 wt.% ZnO.

ABSTRACT

The effects of zinc oxide (ZnO) additive on the crystal structure, densification, and electrical conductivity of the GdSmZr$_2$O$_7$ ceramic have been examined. The GdSmZr$_2$O$_7$ ceramic with and without the addition of 1 wt.% ZnO sintered at temperatures between 1773 and 1973 K exhibits a single cubic pyrochlore-type phase. ZnO is very effective as a sintering aid for the GdSmZr$_2$O$_7$ ceramic, and it reduces the sintering temperature by about 200 K with a positive effect on the total conductivity. The total conductivity of the ZnO-modified GdSmZr$_2$O$_7$, as measured by A.C. impedance spectroscopy under an air atmosphere, is higher than that of the unmodified GdSmZr$_2$O$_7$ at identical temperature levels. At 1173 K, the highest total conductivity of the ZnO-modified GdSmZr$_2$O$_7$ is about fifteen percent higher than that of the un-modified GdSmZr$_2$O$_7$. The 1 wt.% ZnO-modified GdSmZr$_2$O$_7$ is one of good oxide-ion conductors in the oxygen partial pressure range of 1.0×10^{-4} to 1.0 atm at different test temperatures.

© 2013 Elsevier B.V. All rights reserved.

1. Introduction

Solid oxide fuel cells (SOFCs) as one kind of energy conversion devices, which can directly convert chemical energy into electrical energy, have received much attention due to high energy conversion efficiency, little environmental impact, and high fuel flexibility [1–4]. Generally, SOFCs consist of three main components, a porous cathode, a porous anode and an oxide-ion conducting ceramic electrolyte membrane. Traditional 8 mol.% yttria-stabilized zirconia (YSZ) is the most widely used electrolyte material owing to its high ionic conductivity and negligible electron conduction within wide oxygen pressure ranges [5–7]. The standard cathode material for today's SOFCs is perovskite-type La$_{1-x}$Sr$_x$MnO$_3$, and the corresponding anode material is Ni–YSZ cermet [8–10]. However, SOFCs originally operating at high temperatures, typically at above 1123 K, which may lead to destructive chemical reactions at the electrolyte/cathode interface, and may eventually result in the formation of a new resistive layer containing La$_2$Zr$_2$O$_7$ and SrZrO$_3$ phases [11,12]. The resistive layer causes the decrease of the electrical conductivity, and leads to a rapid degradation of the SOFCs' performance. In recent years, the research efforts focus on the increase of the electrical conductivity and the decrease of the electrolyte thickness to reduce the ohmic loss. Therefore, new solid oxide electrolytes or optimized design of electrolytes with a high electrical conductivity are critically important [13–16].

Rare-earth zirconates of the form A$_2$Zr$_2$O$_7$ (A = lanthanide) with a pyrochlore-type or a defect fluorite-type structure, show high chemical stability, high catalytic activity, high radiation tolerance, low thermal conductivity and excellent ionic conductivity [17]. Therefore, rare-earth zirconates are emerging as an important class of solid oxide materials with a number of potential applications as oxide-ion conductors, ceramic thermal barrier coatings, nuclear waste storage materials, and catalysts [18–21]. Recently, great

* Corresponding authors. Tel./fax: +86 451 86414291.
E-mail addresses: zgliu@hit.edu.cn (Z.-G. Liu), ouyangjh@hit.edu.cn (J.-H. Ouyang).
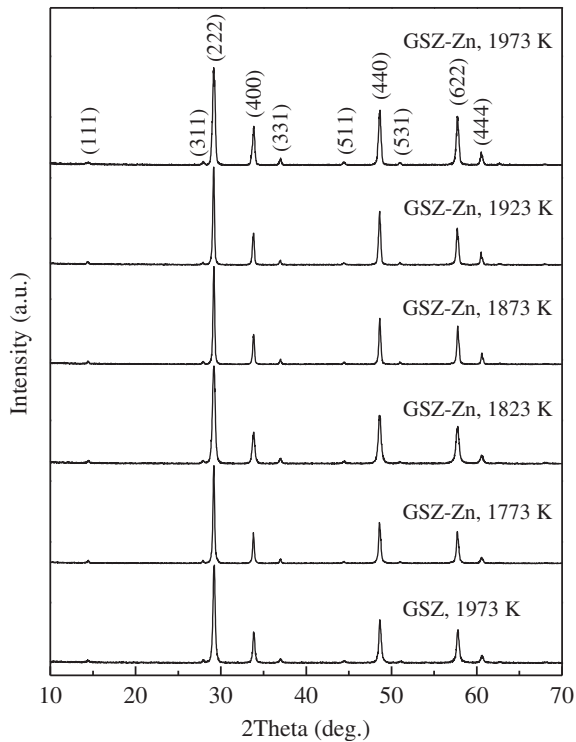
Fig. 1. XRD patterns of the GdSmZr$_2$O$_7$ ceramic with and without the addition of 1 wt.% ZnO sintered at different temperatures for 10 h in air.

oxide electrolytes, such as yttria doped ceria, yttrium-doped barium zirconate and tetravalent metal pyrophosphates [24–26]. In the present work, the GdSmZr$_2$O$_7$ ceramic with or without the addition of 1 wt.% ZnO was prepared by pressureless-sintering method under different sintering temperatures. The effects of the ZnO addition on the crystal structure, densification, and electrical conductivity of the GdSmZr$_2$O$_7$ ceramic were evaluated.

2. Experimental procedure

Polycrystalline gadolinium–samarium zirconate (GdSmZr$_2$O$_7$) ceramic, with or without a small amount (1 wt.%) of ZnO sintering aid (designated with the sample codes of GSZ–Zn and GSZ, respectively), was prepared by the conventional ceramic route using the starting materials Gd$_2$O$_3$ (Rare-Chem Hi-Tech Co., Ltd, China; purity ≥ 99.99%), Sm$_2$O$_3$ (Rare-Chem Hi-Tech Co., Ltd, China; purity ≥ 99.99%), ZrO$_2$ (Dongguan SG Ceramics Technology Co., Ltd, China; purity ≥ 99.9%) and ZnO (Sinopharm Chemical Reagent Co., Ltd, China; purity ≥ 99.9%) powders. The raw materials were calcined at 1173 K for 2 h in air prior to weighing, and were weighed according to the stoichiometry of the samples. An ethanol-based suspension of mixed powders was ball-milled for 24 h using zirconia balls. The mixtures were then dried at 373 K in air. The dried powders were pressed into cylindrical pellets of 13 mm in diameter and about 3 mm in thickness via uniaxial pressing at 20 MPa, followed by isostatic pressing at 200 MPa. Pressureless sintering was carried out at temperatures between 1773 and 1973 K for 10 h under a stagnant air atmosphere.

concerns can be found in the enhancement of the electrical conductivity of A$_2$Zr$_2$O$_7$-type oxides by doping different metal cations [13,22,23]. The GdSmZr$_2$O$_7$ ceramic has the highest electrical conductivity in the (Gd$_{1-x}$Sm$_x$)$_2$Zr$_2$O$_7$ (0 ≤ x ≤ 1.0) series from 623 to 873 K in air [22]. In addition, the GdSmZr$_2$O$_7$ ceramic doped by 15 mol.% MgO exhibits a higher electrical conductivity than the undoped GdSmZr$_2$O$_7$ ceramic at 1173 K in air [23]. However, the refractory nature of rare-earth zirconates including the GdSmZr$_2$O$_7$ ceramic leads to a low sinterability, and generally needs a high sintering temperature (beyond 1973 K) and a long sintering time (more than 10 h) to obtain fully densified pellets [13,18,19,22,23].

It should be noted that the sintering condition has a critical influence on the electrical conductivity of solid oxide electrolytes. It is well known that ZnO is an effective sintering aid for some solid
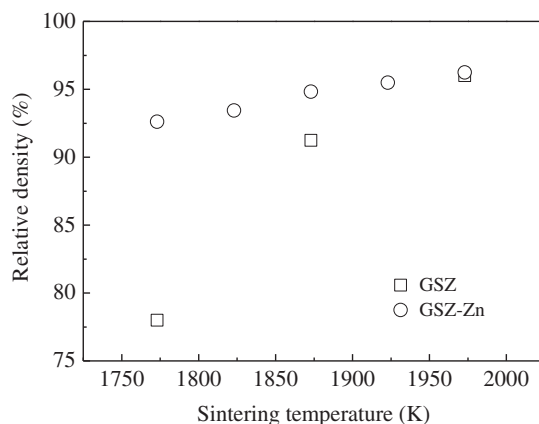

Fig. 2. Relative density of the GdSmZr$_2$O$_7$ ceramic with and without the addition of 1 wt.% ZnO sintered at different temperatures for 10 h in air.

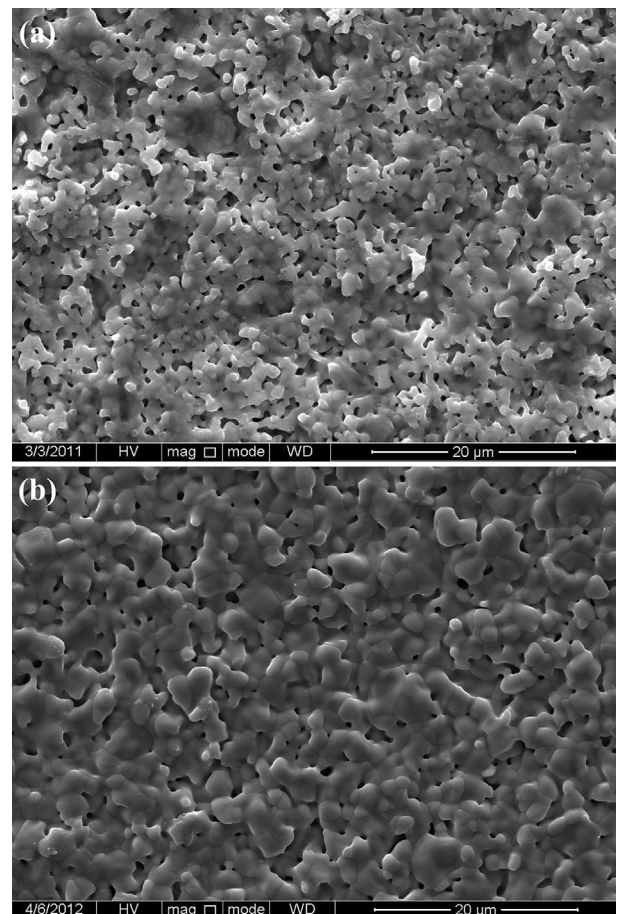**Fig. 3.** SEM surface images of the GdSmZr$_2$O$_7$ ceramic with and without the addition of 1 wt.% ZnO sintered at 1773 K for 10 h in air: (a) GSZ, (b) GSZ–Zn.

X-ray diffraction (XRD) patterns were recorded to identify the crystalline phase of sintered samples by a Rigaku D/Max 2200VPC diffractometer using Ni-filtered Cu Kα radiation at 40 kV and 30 mA. The data were recorded between 10° and 70° with a step size of 0.02° and a scanning rate of 5° min^{-1}. The densities of sintered samples were measured by the usual volume and weight measurement technique. The surface morphology of sintered samples was observed using a field-emission scanning electron microscope (FEI Quanta 200F, the Netherlands). To obtain better image resolution, a thin gold film was deposited onto the surfaces of sintered samples by radio frequency sputtering.

For impedance spectroscopic studies, a high-temperature-curing platinum paste was applied on polished parallel faces of the pellets with the dimensions of 8 mm in diameter and 1 mm in thickness. The pellets were then electroded with long platinum wires. The electroded pellets were cured in an air furnace for 2 h at 1223 K. Impedance measurements of the pellets were carried out from 773 to 1173 K in the frequency range of 40 Hz to 4 MHz using a computer-controlled impedance analyzer (Solartron™ SI 1260, UK). The effect of oxygen partial pressure (p_{O_2}) on the electrical conductivity of pellets was investigated in a closed tube furnace cell. The oxygen partial pressure in the chamber was monitored with an yttria-stabilized zirconia sensor, and was kept from around 1.0×10^{-4} to 1.0 atm with a N_2–O_2 gas mixture. The impedance data were fitted using Zview™ software.

3. Results and discussion

Fig. 1 shows the XRD patterns of the GdSmZr$_2$O$_7$ ceramic with and without the addition of 1 wt.% ZnO. All observed diffraction peaks can be well indexed with an ideal cubic pyrochlore-type structure belonging to the Fd3m space group symmetry. Pyrochlore is a superstructure of a cubic fluorite-type unit cell, which has a typical face-centered-cubic arrangement of cations with anions in the tetrahedral holes. The diffraction patterns exhibit a series of relatively weak characteristic peaks of the pyrochlore superlattice, e.g., (111), (311), (331), (511), and (531) [13,18,27]. Fig. 2 displays the relative density of the GdSmZr$_2$O$_7$ ceramic with and without the addition of 1 wt.% ZnO sintered at various temperatures with soaking time of 10 h in air. It is clearly seen that the relative density of the GdSmZr$_2$O$_7$ ceramic with and without the addition of 1 wt.% ZnO increases with increasing the sintering temperature. The relative density of the ZnO-modified GSZ sintered at 1773 K zooms to 92.6%, whereas the relative density of the unmodified GSZ sintered at 1773 K is only 78.0%. It indicates that ZnO is very effective as a sintering aid for the GdSmZr$_2$O$_7$ ceramic.

Fig. 3 shows the SEM surface images of the GdSmZr$_2$O$_7$ ceramic with and without the addition of 1 wt.% ZnO sintered at 1773 K for 10 h in air. The unmodified GSZ is found to be very porous, and the pores are continuous and open. In contrast, the ZnO-modified GSZ is quite dense, which is in agreement with the above density results. In addition, the grains of the ZnO-modified GSZ are polygonal with a heterogeneous distribution, and the grain boundaries are very clean. No second phase is found in Fig. 3(b), which is consistent with the above XRD results.

Fig. 4(a–f) illustrates the complex impedance plots obtained for the GdSmZr$_2$O$_7$ ceramic with and without the addition of 1 wt.% ZnO during impedance measurements at 773 K. The impedance spectra are fitted on assuming a series association of parallel resistance and constant phase element (CPE), as shown in Fig. 4(g).

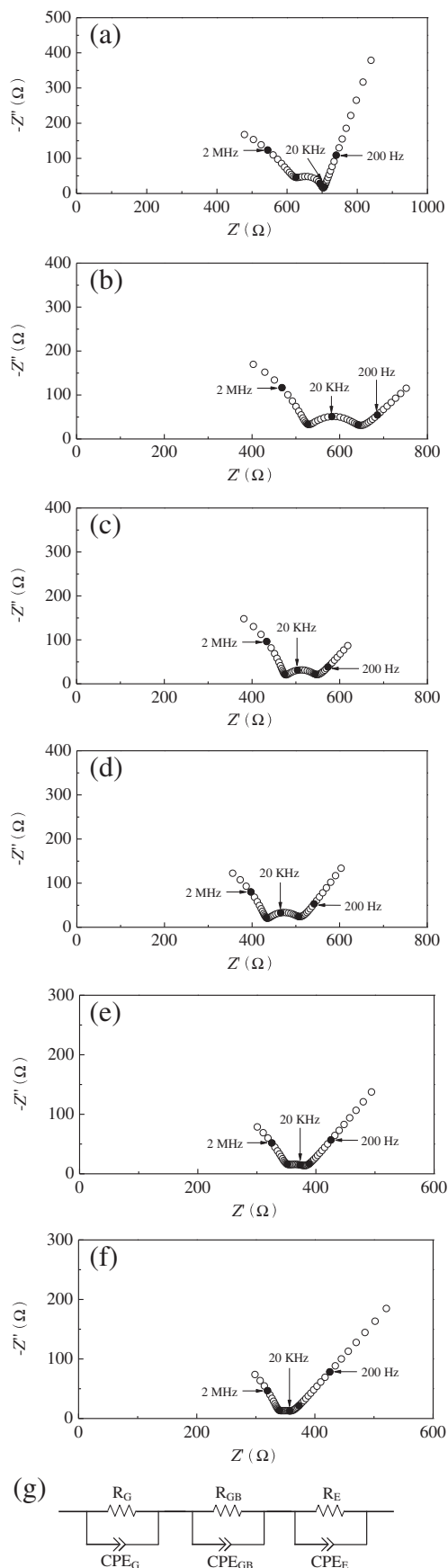**Fig. 4.** Complex impedance spectra and schematic equivalent electrical circuit plot of the GdSmZr$_2$O$_7$ ceramic with and without the addition of 1 wt.% ZnO at 773 K in air: (a) GSZ sintered at 1973 K, (b) GSZ–Zn sintered at 1773 K, (c) GSZ–Zn sintered at 1823 K, (d) GSZ–Zn sintered at 1873 K, (e) GSZ–Zn sintered at 1923 K, (f) GSZ–Zn sintered at 1973 K, (g) equivalent electrical circuit.
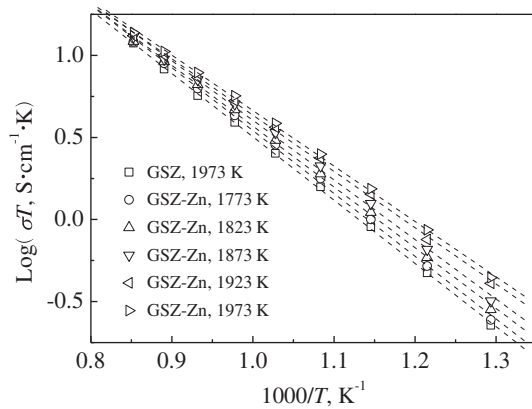
Fig. 5. Arrhenius plots of the total conductivity of the GdSmZr$_2$O$_7$ ceramic with and without the addition of 1 wt.% ZnO.

Due to the inhomogeneity of microstructure within the sintered samples, the capacitance is replaced by CPE [28]. The three obvious contributions from the high frequency to the low frequency are those from grain, grain boundary and electrode polarization, respectively. From the impedance spectra, grain resistance (R_G) and grain-boundary resistance (R_{GB}) can be obtained. The total resistance (R_T) is given by $R_T = R_G + R_{GB}$. The errors of grain resistance and grain boundary resistance between the experimental measurements and the fit results from the equivalent circuit model in Fig. 4(g) using Zview™ software are both less than 1.0%. It is clearly seen that the unmodified GSZ exhibits a higher total resistance than the ZnO-modified GSZ. It is also significant that the sizes of the grain arcs are larger than those of the grain boundary ones.

Fig. 5 shows the temperature dependence of the total conductivity of the GdSmZr$_2$O$_7$ ceramic with and without the addition of 1 wt.% ZnO. The total conductivity is found to follow the Arrhenius behavior given by the following equation,

$$\sigma \cdot T = \sigma_0 \exp(-E/k_B T) \tag{1}$$

where σ_0 is the pre-exponential factor, which is a measurement of the effective number of mobile oxide ions, E denotes the activation energy for the conduction process, K_B is Boltzmann constant, and T is the absolute temperature. The straight dotted lines in Fig. 4(a–f) are the least-square linear fitting of the total conductivity at various sintering temperatures. It is important to note that the use of a single straight line is sufficient to fit the total conductivity in the whole temperature range (773–1173 K) in the present work, with typical correlation coefficients for linear least squares fit over 0.9995 for all linear fittings. Clearly, the total conductivity of the GdSmZr$_2$O$_7$ ceramic with and without the addition of 1 wt.% ZnO gradually increases with increasing the test temperature from 773 to 1173 K. The activation energies for the total conductivity of the GdSmZr$_2$O$_7$ ceramic with and without the addition of 1 wt.% ZnO, calculated from a fit of the data to the Arrhenius equation, are listed

Table 1
Activation energies for the total conductivity of the GdSmZr$_2$O$_7$ ceramic with and without the addition of 1 wt.% ZnO.

Samples	Activation energies (eV)
GSZ sintered at 1973 K	0.765 ± 0.005
GSZ–Zn sintered at 1773 K	0.759 ± 0.009
GSZ–Zn sintered at 1823 K	0.735 ± 0.009
GSZ–Zn sintered at 1873 K	0.720 ± 0.012
GSZ–Zn sintered at 1923 K	0.680 ± 0.009
GSZ–Zn sintered at 1973 K	0.670 ± 0.008

Table 2
Total conductivities of the GdSmZr$_2$O$_7$ ceramic with and without the addition of 1 wt.% ZnO at typical test temperatures.

Samples	773 K ($\times 10^{-4}$ S cm^{-1})	973 K ($\times 10^{-3}$ S cm^{-1})	1173 K ($\times 10^{-2}$ S cm^{-1})
GSZ sintered at 1973 K	2.93	2.60	1.01
GSZ–Zn sintered at 1773 K	3.16	2.93	1.03
GSZ–Zn sintered at 1823 K	3.66	3.13	1.04
GSZ–Zn sintered at 1873 K	4.12	3.48	1.11
GSZ–Zn sintered at 1923 K	5.28	3.75	1.12
GSZ–Zn sintered at 1973 K	5.72	3.96	1.17

in Table 1, which are in the order of those previously reported values in similar rare-earth zirconate systems with a pyrochlore-type structure [22,23]. It is also seen that the activation energy for the total conductivity of the ZnO-modified GSZ slightly decreases with increasing the sintering temperature from 1773 to 1973 K, correspondingly ranging between 0.760 and 0.675 eV. The average grain size of the ZnO-modified GdSmZr$_2$O$_7$ gradually increases with increasing the sintering temperature. The grain boundary area in ZnO-modified GdSmZr$_2$O$_7$ decreases with increasing the average grain size. Since the grain boundary generally blocks the conduction process, the decrease in the grain boundary area is beneficial to the improvement of the total conductivity of the ZnO-modified GdSmZr$_2$O$_7$. Therefore, the total conductivity gradually increases with increasing the sintering temperature, while the activation energy slightly decreases.

Total conductivities of the GdSmZr$_2$O$_7$ ceramic with and without the addition of 1 wt.% ZnO at typical test temperatures are listed in Table 2, and the errors derived from the resistance measurements are less than 2.0%. Obviously, the total conductivity of the ZnO-modified GSZ sintered at 1773 K is comparable to that of the unmodified GSZ sintered at 1973 K. It indicates that ZnO is an effective sintering aid for the GdSmZr$_2$O$_7$ ceramic, reducing the sintering temperature by about 200 K and greatly enhancing the densification process, with a positive effect on the total conductivity of the GdSmZr$_2$O$_7$ ceramic. In the present work, the highest total conductivity of the ZnO-modified GSZ is 1.17×10^{-2} S cm^{-1} at 1173 K, which is about fifteen percent higher than that of the unmodified GSZ.
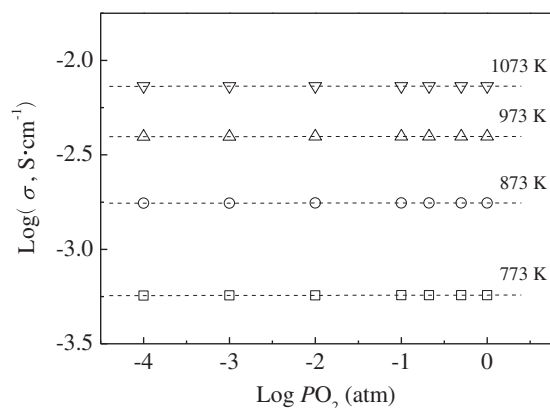

Fig. 6. Oxygen partial pressure dependence of the total conductivity of the ZnO-modified GSZ sintered at 1973 K in air.

The oxygen partial pressure (p_{O_2}) dependence of the total conductivity was measured in order to clarify the conduction carrier of the GdSmZr$_2$O$_7$ ceramic with and without the addition of 1 wt.% ZnO. Fig. 6 shows the total conductivity of the ZnO-modified GSZ sintered at 1973 K as a function of oxygen partial pressure at different test temperatures. Clearly, the total conductivity of the ZnO-modified GSZ sintered at 1973 K is almost independent of oxygen partial pressure from 1.0×10^{-4} to 1.0 atm at different test temperatures, which indicates that the conduction of the ZnO-modified GSZ sintered at 1973 K is purely ionic with negligible electronic conduction [29]. In consideration of the total conductivity of the ZnO-modified GSZ being slightly lower than that of conventional solid electrolytes such as yttria-stabilized zirconia (YSZ), samaria/gadolinia-doped ceria (SDC/GDC), strontium- and magnesium-doped lanthanum gallate (LSGM), and bismuth oxide (BiO$_{1.5}$)-based electrolytes, the most likely applications of the ZnO-modified GSZ in SOFCs are high-temperature solid oxide electrolytes, or thick-film electrolytes, or protective layers applied onto CeO$_2$- or LaGaO$_3$-based solid oxide electrolytes [30].

4. Conclusions

The GdSmZr$_2$O$_7$ ceramic with and without the addition of 1 wt.% ZnO sintered at temperatures between 1773 and 1973 K exhibits a single cubic pyrochlore-type phase. The relative density of the GdSmZr$_2$O$_7$ ceramic with or without the addition of 1 wt.% ZnO increases with increasing the sintering temperature. ZnO is very effective as a sintering aid for the GdSmZr$_2$O$_7$ ceramic, and it reduces the sintering temperature by about 200 K with a positive effect on the total conductivity. The total conductivity of the ZnO-modified GSZ is higher than that of the unmodified GSZ at identical temperature levels. At 1173 K, the highest total conductivity of the ZnO-modified GSZ is about fifteen percent higher than that of the unmodified GSZ. The 1 wt.% ZnO-modified GSZ is one of good oxide-ion conductors in the oxygen partial pressure range of 1.0×10^{-4} to 1.0 atm at different test temperatures.

Acknowledgments

References

[1] L. Malavasi, C.A.J. Fisherb, M.S. Islam, Chem. Soc. Rev. 39 (2010) 4370–4387.
[2] K.S. Howe, G.J. Thompson, K. Kendall, J. Power Sources 196 (2011) 1677–1686.
[3] X.D. Zhou, S.C. Singhal, Struct. Bond. 141 (2011) 1–32.
[4] M.A. Laguna-Bercero, J. Power Sources 203 (2012) 4–16.
[5] J.W. Fergus, J. Power Sources 162 (2006) 30–40.
[6] E. Courtin, P. Boy, C. Rouhet, L. Bianchi, E. Bruneton, N. Poirot, C. Laberty-Robert, C. Sanchez, Chem. Mater. 24 (2012) 4540–4548.
[7] E. Courtin, P. Boy, T. Piquero, J. Vulliet, N. Poirot, C. Laberty-Robert, J. Power Sources 206 (2012) 77–83.
[8] E. Fabbri, D. Pergolesi, E. Traversa, Sci. Technol. Adv. Mater. 11 (2010) 044301.
[9] H.J. Park, Z. Shao, W. Wang, K.S. Moon, Fuel Cells 11 (2011) 654–660.
[10] Z. Zhao, L. Liu, X.M. Zhang, W.M. Wu, B.F. Tu, D.R. Ou, M.J. Cheng, J. Power Sources 222 (2013) 542–553.
[11] A. Chen, G. Bourne, K. Siebein, R. DeHoff, E. Wachsman, K. Jones, J. Am. Ceram. Soc. 91 (2008) 2670–2675.
[12] N. Li, M.K. Mahapatra, P. Singh, J. Power Sources 221 (2013) 57–63.
[13] Z.-G. Liu, J.-H. Ouyang, K.-N. Sun, X.-L. Xia, Electrochim. Acta 55 (2010) 8466–8470.
[14] X.L. Zhou, L.M. Liu, J.M. Zhen, S.C. Zhu, B.W. Li, K.N. Sun, P. Wang, J. Power Sources 196 (2011) 5000–5006.
[15] J.R.S. Pereira, S. Rajesh, F.M.L. Figueiredo, F.M.B. Marques, Electrochim. Acta 90 (2013) 71–79.
[16] W. Liu, S. Yamaguchi, T. Tsuchiya, S. Miyoshi, K. Kobayashi, W. Pan, J. Power Sources 235 (2013) 62–66.
[17] M.A. Subramanian, G. Aravamudan, G.V. Subba Rao, Prog. Solid State Chem. 15 (1983) 55–143.
[18] Z.-G. Liu, J.-H. Ouyang, K.-N. Sun, X.-L. Xia, J. Power Sources 195 (2010) 7225–7229.
[19] Z.-G. Liu, J.-H. Ouyang, Y. Zhou, S. Li, J. Eur. Ceram. Soc. 30 (2010) 2707–2713.
[20] G. Sattonnay, C. Grygiel, I. Monnet, C. Legros, M. Herbst-Ghysel, L. Thomé, Acta Mater. 60 (2012) 21–34.
[21] S. Gaur, D.J. Haynes, J.J. Spivey, Appl. Catal. A – Gen. 403 (2011) 142–151.
[22] Z.-G. Liu, J.-H. Ouyang, Y. Zhou, X.-L. Xia, J. Power Sources 185 (2008) 876–880.
[23] Z.-G. Liu, J.-H. Ouyang, K.-N. Sun, Y. Zhou, Adv. Appl. Ceram. 111 (2012) 214–219.
[24] L. Gao, M. Zhou, Y.F. Zheng, H.T. Gu, H. Chen, L.C. Guo, J. Power Sources 195 (2010) 3130–3134.
[25] P. Babilo, S.M. Haile, J. Am. Ceram. Soc. 88 (2005) 2362–2368.
[26] J. Xiao, H.M. Zhang, Z.J. Yang, H.T. Wang, G.L. Ma, Z.F. Zhou, J. Alloys Compd. 521 (2012) 106–111.
[27] Z.H. Xu, S.M. He, L.M. He, R.D. Mu, G.H. Huang, X.Q. Cao, J. Alloys Compd. 509 (2011) 4273–4283.
[28] J.R. Macdonald, W.B. Johnson, in: E. Barsoukov, J.R. Macdonald (Eds.), Impedance Spectroscopy: Theory, Experiment and Applications, second ed., John Wiley & Sons, Inc., New Jersey, 2005, pp. 1–26.
[29] J.B. Goodenough, Annu. Rev. Mater. Res. 33 (2003) 91–128.
[30] V.V. Kharton, F.M.B. Marques, A. Atkinson, Solid State Ionics 174 (2004) 135–149.